On numerical broadening of particle size spectra:
a condensational growth study using PyMPDATA 1.0

Michael Olesik[1], Sylwester Arabas[1], Jakub Banaśkiewicz[1], Piotr Bartman[1], Manuel Baumgartner[2,3], and Simon Unterstrasser[4]

[1]Jagiellonian University, Kraków, Poland
[2]Zentrum für Datenverarbeitung, Johannes Gutenberg University Mainz, Germany
[3]Institute for Atmospheric Physics, Johannes Gutenberg University Mainz, Germany
[4]German Aerospace Center (DLR), Oberpfaffenhofen, Germany

Correspondence: Michael Olesik (michael.olesik@doctoral.uj.edu.pl)

Abstract. The work discusses the diffusional growth in particulate systems such as atmospheric clouds. It focuses on the Eulerian modeling approach in which the evolution of the probability density function describing the particle size spectrum is carried out using a fixed-bin discretization. The numerical diffusion problem inherent to the employment of the fixed-bin discretization is scrutinized. The work focuses on the applications of MPDATA family of numerical schemes. Several MPDATA variants are explored including: infinite-gauge, non-oscillatory, third-order-terms and recursive antidiffusive correction (double pass donor cell, DPDC) options. Methodology for handling coordinate transformations associated with both particle size distribution variable choice and numerical grid layout are expounded. The study uses PyMPDATA - a new open-source Python implementation of MPDATA. Analysis of the performance of the scheme for different discretization parameters and different settings of the algorithm is performed using an analytically solvable test case pertinent to condensational growth of cloud droplets. The analysis covers spatial and temporal convergence, computational cost, conservativeness and quantification of the numerical broadening of the particle size spectrum. Presented results demonstrate that, for the problem considered, even a tenfold decrease of the spurious numerical spectral broadening can be obtained by a proper choice of the MPDATA variant (maintaining the same spatial and temporal resolution).

1 Introduction

1.1 Motivation and outline

The focus of this paper is on the problem of predicting the particle size evolution for a population of droplets undergoing diffusional growth. Embracing continuous description of the particle size spectrum using a number density function, the problem can be stated using a population-balance equation expressing conservation of number of particles. Herein, the numerical solution of the problem using the MPDATA family of finite difference schemes originating in Smolarkiewicz (1983, 1984) is discussed. MPDATA stands for Multidimensional Positive Definite Advection Transport Algorithm and is a higher-order iterative extension of the forward-in-time upwind scheme.

MPDATA features a variety of options allowing to pick an algorithm variant appropriate to the problem at hand. This work highlights the importance of MPDATA algorithm variant choice for the resultant spectral broadening of the particle size spectrum.

25   The term spectral broadening refers to the increasing width of the droplet spectrum during the lifetime of a cloud, which may be associated with both physical mechanisms (mixing, turbulence) as well as spurious artifacts stemming from the employed numerical solution technique.

Cloud simulations with detailed treatment of droplet microphysics face a twofold challenge in prognosing the droplet spectrum width. First, it is challenging to model and numerically represent the subtleties of condensational growth (e.g., Arabas
30   and Shima, 2017; Yang et al., 2018), even more so when considering the interplay between particle population dynamics and supersaturation fluctuations (e.g., Jeffery et al., 2007; Abade et al., 2018). Second, the discretization strategies employed in representing the particle size spectrum and its evolution are characterized by inherent limitations which constrains the fidelity of spectral width predictions (e.g., Arabas and Pawlowska, 2011; Morrison et al., 2018). Finally, corroboration of spectral width estimates from both theory and modeling against experimental data faces the problems of instrumental broadening inherent to
35   the measurement techniques (e.g. Devenish et al., 2012, sec. 3.2) and the problem of sampling volume choice (e.g., Kostinski and Jameson, 2000).

The width of the spectrum plays a key role in the determination of both the droplet collision probabilities Grabowski and Wang (2013) and the characteristics relevant for radiative-transfer (Chandrakar et al., 2018). Consequently, it is of high interest to disentangle the size effects on the droplet spectrum that come from the exact solution of the governing equation or are a
40   consequence of the numerical discretization (i.e. numerical diffusion).

The following introductory subsections start with a literature review of applications of finite-difference schemes, and MPDATA in particular, to the problem of condensational growth of population of particles.

Section 2 contains a tutorial on MPDATA variants and is limited to one-dimensional homogeneous advection of a positive-sign signal. It is presented with the aim of gathering information that is scattered across works focusing on more complex
45   computational fluid dynamics applications of MPDATA. Example simulations employing an analytically solvable test case pertaining to the evolution of cloud droplet size spectrum in a cumulus cloud is used to depict the effects on numerical broadening from enabling the discussed algorithm variants. While comprehensive from the point of view of the considered problem of diffusional growth, the presented material merely hints the versatility of the algorithm. For a proper review of MPDATA family of algorithms highlighting the multi-dimensional aspects and its multifaceted applications, see Margolin and Smolarkiewicz
50   (1998); Smolarkiewicz (2006); Kühnlein and Smolarkiewicz (2017).

Section 3 documents analyses of spectral broadening and mass conservativeness. An analysis of the computational cost of different algorithm variants is carried out and corroborated with previously published data.

Section 4 concludes the work with a summary of findings.

Appendix A contains convergence analysis based on results of multiple simulations using the embraced test case run with
55   different temporal and spatial resolutions.

1.2 Background

There exist two contrasting approaches for modeling the evolution of cloud droplet size spectrum (see Grabowski, 2020, for a review): Eulerian (fixed bin) and the Lagrangian (particle based or moving bin). The Lagrangian approach has the advantages of: (i) simplicity of formulation (no need to define particle-level properties and processes as gridded continuous fields),
60 (ii) lack of discretization-related artifacts such as numerical diffusion associated with solving PDEs, (iii) facilitation of tracking multiple particle attributes such as the amount of solute required for modeling activation. On the other hand, there are inherent challenges in using the particles-based framework: (i) ensuring proper sampling of physical and parameter space, (ii) handling load-balancing in distributed memory environments, (iii) solvability of resultant stiff ODE systems. Overall, while the Lagrangian methods are the focus of active research and development (Grabowski et al., 2019), the Eulerian schemes have been
65 predominantly used in large scale modeling (Khain et al., 2015), due to their consistency with the fluid advection dynamics description and due to robust algorithms for representing particle collisions.

Following Liu et al. (1997) and Morrison et al. (2018), the earliest documented study employing Eulerian numerics for condensational growth of a continuous size distribution representing a population of particles is that of Kovetz and Olund (1969) (whereas several earlier works starting with Howell (1949) utilized the Lagrangian approaches). The numerical scheme
70 proposed in Kovetz and Olund (1969, eq. (10)) resembles an upwind algorithm being explicit in time and orienting the finite-difference stencil differently for condensation and evaporation.

Likely one of the first discussions of numerical broadening of the spectrum can be found in Brown (1980) where the numerical scheme from Kovetz and Olund (1969) was improved in several ways, including sampling of the drop growth rate at the bin boundaries (as is done here). Their study also covers quantification of the error of the method by comparisons to analytic
75 solutions.

In Tsang and Brock (1982), the authors point out that upwind differencing is not suitable for aerosol growth calculations for its unacceptable numerical diffusion. Noteworthy, the study includes considerations of the Kelvin effect of surface tension on the drop growth (not considered herein).

The first mention of application of MPDATA for the problem of condensational growth can be found already in Smo-
80 larkiewicz (1984) where the problem is given as an example where the divergent-flow option of the algorithm may be applicable (see sect. 2.6 below).

In Tsang and Korgaonkar (1987), which is focused on the evaporation of an "aerosol cloud", MPDATA is used as a predictor step followed by a corrective step using a Galerkin finite element solver. In two subsequent studies from the same group (Tsang and Rao, 1988, 1990), MPDATA is compared with other algorithms in terms of mass conservation, number conservation and
85 computational cost. In Tsang and Rao (1988), basic 3-iteration MPDATA is used, although interestingly it is noted there that "*If the antidiffusion velocities are increased by some factor between 1.04 and 1.08, use of [corrective iteration] only once can reduce 50% of the computing time [...] without much sacrifice of accuracy*". In conclusions, the authors praise MPDATA for providing narrow size distributions. At the same time, it is pointed out that MPDATA performs worse than upwind in terms of mass conservation or mean radius prediction accuracy.

The "Aerosol Science: Theory and Practice" book of Williams and Loyalka (1991) contains a section on MPDATA within Chapter 5 focusing on the methods of solving the dynamic equation describing aerosol spectrum evolution. The basic variant of MPDATA (Smolarkiewicz, 1983) is presented with an outline of its derivation.

In Kostoglou and Karabelas (1995) and Dhaniyala and Wexler (1996) the authors mention that MPDATA has the potential to reduce errors in size computations. The latter work lists high computational cost among drawbacks in using the algorithm that led to discarding the scheme from the presented comparison.

In Morrison et al. (2018), a comparison of different numerical schemes for condensational growth problem is performed. Both fixed-, and moving-bin approaches are compared, including the non-oscillatory variant of MPDATA (referred to as MPDG therein). MPDATA is reported to produce significant numerical diffusion and spectral broadening relative to all other methods. Intriguingly, as can be seen in Fig. 7 therein, the broad spectrum in the results obtained with MPDATA appears already at the very beginning of the simulations presented (at the altitude of 20m out of 520m of simulated displacement of an air parcel). Overall, the discussion in Morrison et al. (2018), focuses on the issue of spectral broadening from vertical numerical diffusion highlighting that, in principle, the problem is a four-dimensional transport problem (three spatial dimensions and the spectral dimension).

In Wei et al. (2020), MPDATA is employed for integrating droplet spectrum evolution for comparison with a Lagrangian scheme. The work concludes that the spurious broadening of the spectrum cannot be alleviated even with a grid composed of 2000 size bins.

Noteworthy, none of the works mentioned above discussed coordinate transformations to non-linear grid layouts with MP-DATA (a discussion of handling non-uniform mesh with upwind scheme can be found in Li et al., 2017, Appendix A). Wei et al. (2020) and Morrison et al. (2018) are the only works mentioning other than basic flavor of the scheme, yet only the non-oscillatory option was considered. Herein, the applicability of multiple variants of MPDATA and their combinations is expounded highlighting their robustness for solving the condensational growth problem.

1.3 Governing equations

To describe the conservation of particle number N under the evolution of the particle size spectrum $n_p(p) = \frac{dN}{dp}$ (n denoting number density as a function of particle size parameter p such as radius or volume), one may take the one-dimensional continuity equation (i.e., Liouville equation expressing the conservation of probability, for discussion see Hulburt and Katz, 1964), in a generalized coordinate system:

$$\partial_t(Gn_p) + \partial_x(uGn_p) = 0, \tag{1.1}$$

where $G \equiv G(x)$ represents the coordinate transformation from p to x, x being an equidistant mesh coordinate used in the numerical solution; $n_p \equiv n_p(p(x))$ being number density function and $u \equiv u(x)$ denoting the pace of particle growth in the chosen coordinate x. The coordinate transformation term G may play a twofold role in this context. First, there is a degree of freedom in the choice of the particle-size parameter used as the coordinate (i.e., the argument p of the density function $n(p)$). For the chosen coordinates $p \in [r, s \sim r^2, v \sim r^3]$, the appropriate distributions will be $n_r(r)$, $n_s(s)$ and $n_v(v)$ where $s = 4\pi r^2$

and $v = 4/3\pi r^3$ denote particle surface and volume, respectively. The size spectrum $n_p(p)$ in a given coordinate is related with $n_r(r)$ via the following relation of measures: $n_p(p)dp = n_r(r)dr$ so the total number $N = \int n_r dr$ is conserved.

125   Second, there is also a degree of freedom in the choice of the grid layout $p(r(x))$, that is how the parameters r, s or v are discretized to form the equidistant grid in x. This can be used, for instance, to define a mass-doubling grid layout ($x = \ln_2(r^3)$) as used in Morrison et al. (2018) and herein.

Combining the two transformations results in the following definition of G:

$$G \equiv dp(r)/dx(r) = \frac{dp}{dx} \tag{1.2}$$

130   which defines the transformation from the coordinate p of the density function to the numerical mesh coordinate x. For further discussion of the coordinate transformation approaches in the embraced framework (including multi-dimensional setting), see Smolarkiewicz and Clark (1986) and Smolarkiewicz and Margolin (1993).

1.4   Upwind discretization

The numerical solution of equation (1.1) will be obtained by discretizing space and time as follows: $x = i \cdot \Delta x$ and $t = n \cdot$
135   Δt. Henceforth, ψ_i^n and G_i denote the discretized number density n_p and the discretized coordinate transformation term, respectively. The dimensionless advective field is denoted by $GC = \frac{dp}{dx}u\Delta t/\Delta x$, where C stands for the Courant number, i.e. the velocity in terms of temporal and spatial grid increments. A staggered grid is employed what warrants introduction of fractional indexing for vector fields, i.e.: $GC_{i+1/2} \equiv (GC)|_{i+1/2}$ in the case of the discretisation of the product GC. To solve the equation numerically, a finite difference form of the differential operators is introduced embracing the so-called upwind
140   approach (dating back at least to Courant et al., 1952, eq. 16 therein):

$$\psi_i^{n+1} = \psi_i^n - \frac{1}{G_i}\left(F(\psi_i^n, \psi_{i+1}^n, GC_{i+1/2}) - \right.$$
$$\left. F(\psi_{i-1}^n, \psi_i^n, GC_{i-1/2})\right) \tag{1.3}$$

with

$$F(\psi_L, \psi_R, GC_{\text{mid}}) = \max(GC_{\text{mid}}, 0) \cdot \psi_L +$$
145
$$\min(GC_{\text{mid}}, 0) \cdot \psi_R \tag{1.4}$$

where the introduced flux function F defines the flux of ψ across grid-cell boundary as a function of the values of ψ_L and ψ_R to the left and right of the boundary, respectively and the value of GC at the boundary. Hereinafter a shorthand notation $F_{i+\frac{1}{2}}(\psi) \equiv F(\psi_i, \psi_{i+1}, GC_{i+\frac{1}{2}})$ is used.

1.5   Test case and upwind solution

150   The test case is based on Figure 3 from East (1957) - one of the early papers on the topic of cloud droplet spectral broadening. The case considers the growth of a population of cloud droplets through condensation in the equilibrium supersaturation limit,

where:

$$u \approx \frac{dx}{dr}\dot{r} = \frac{dx}{dr}\frac{\xi}{r}, \tag{1.5}$$

with $\xi = \xi_0(S-1)$ being an approximately constant factor proportional to supersaturation $(S-1)$. The parameter ξ_0 is set to 100 $\mu m^2 s^{-1}$ to match the results from East (1957).

For the initial number density distribution function, an idealized fair-weather cumulus droplet size spectrum is modeled with a lognormal distribution:

$$n_r^{(0)}(r) = n_0 \exp\left(-\kappa(\log_{10}(r/r_0))^2\right)/r \tag{1.6}$$

with parameters: $r_0 = 7$ μm, $n_0 = 465$ cm^{-3} and $\kappa = 22$.

For the boundary conditions (implemented using halo grid cells), extrapolation is applied for G, while both ψ and GC are set to zero within the halo.

Analytical solution to eq. (1.1) is readily obtainable for $\dot{r} = \xi/r$ and for any initial size distribution. Noting that introducing $x = r^2$ coordinates, the transport equation (1.1) becomes a constant-coefficient advection equation, the problem reduces to translation of the signal in x by $2\xi t$. Cast in the r coordinate, the solution can be expressed as (Kovetz, 1969):

$$\psi^{\text{analytical}} = n_r(r, t > 0) \equiv \frac{r}{\tilde{r}} n_r^{(0)}(\tilde{r}), \tag{1.7}$$

where $\tilde{r} = \tilde{r}(r,t) = \sqrt{r^2 - 2\xi t}$.

The upper panels in Figures 1 and 2 depict the droplet size spectrum evolution through condensational growth from an initial liquid water mixing ratio of $M_0 = 1$ $g\,kg^{-1}$ under supersaturation $S - 1 = 0.075\%$.

Two grid layout (x) and size parameter (p) choices are depicted. Both panels in Fig. 1 present simulation carried out with density function coordinate $p = r^2$ and discretized on a mass-doubling grid $(x = \ln_2(r^3))$, whereas both panels in Fig. 2 present simulation results obtained with $x = r$ and $p = r$. In both cases, the timestep is set to $\Delta t = \frac{1}{3}$ s, the domain range is $(1; 26)$ μm, there are 75 grid cells. Such settings corresponds to $GC \approx 0.26$ in first layout, where $p = r^2$ is used, and variable Courant number approximately in the range of $(0.03; 0.07)$ in second layout, where $p = r$ is used.

The snapshots are depicted at times where the liquid water mixing ratio of the analytical solution obtains values of 1, 4 and 10 $g\,kg^{-1}$ (assuming air density of 1 $kg\,m^{-3}$). In both Figure 1 and 2, the upper panels display the number density and the bottom panel show the normalized mass density. The bottom panels thus depict the same quantities as Fig. 3 in East (1957).

The normalized mass density of bin i is evaluated as $4/3\pi\rho_l m_i^{(l=3)}/M$ by calculating the third statistical moment of the number distribution $n_r(p)$ with the formula:

$$m_i^{(l)} = \int_{r_1}^{r_2} n_r r^l dr =$$

$$= \psi_i \cdot \begin{cases} (l+1)^{-1} r^{l+1}\Big|_{r_1}^{r_2} & \text{for } p = r \\ 2(l+2)^{-1}(r^2)^{\frac{l+2}{2}}\Big|_{r_1^2}^{r_2^2} & \text{for } p = r^2 \end{cases} \tag{1.8}$$
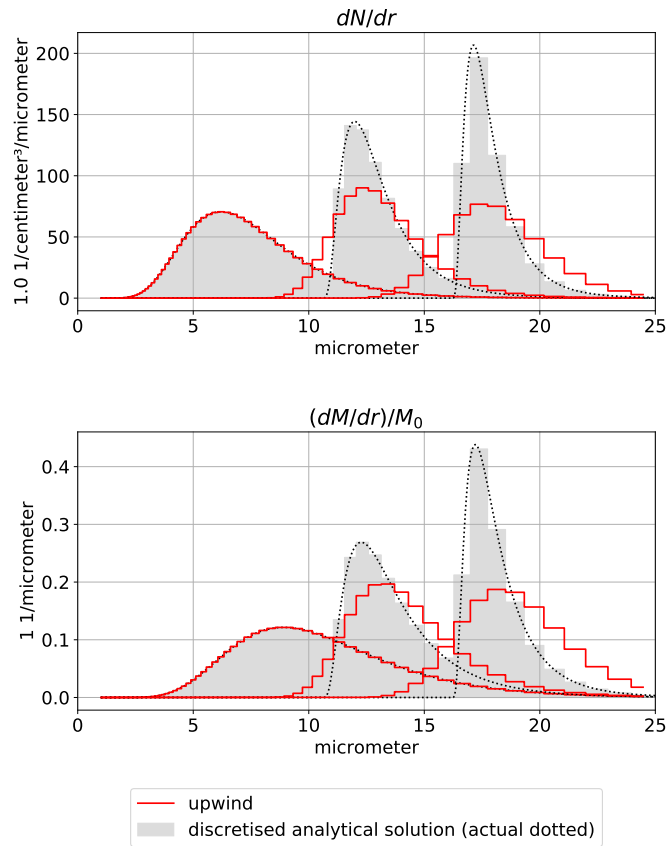
Figure 1. Evolution of the number density (upper panel) and normalized mass density (bottom panel) with red histograms corresponding to the numerical solution using upwind scheme, black dots depicting analytical solution, and gray filled histogram representing discretized analytical solution; compare Fig. 3 in East (1957). Numerical solution was obtained in the following coordinate transformation: $p = r^2$; $x = \ln_2(r^3)$

180   where r_1, r_2 are the boundaries of i-th bin, and ψ_i is the value of n_p associated with the bin (i.e., n_p is assumed to be bin-wise constant; note that the dimension of n_p depends on the choice of p). The normalization factor M is the mixing ratio (e.g., $M = M_0 = 1\,\mathrm{g\,kg^{-1}}$ for $t = 0$).

    The dotted curve corresponds to the analytic solution. The numerical solution obtained with the upwind scheme (1.3) is plotted with red histograms and compared with the discretized analytical solution plotted as grey filled histograms.

185   Looking at the mass density plots in Figs. 1 and 2, it is evident that casting the results in the form of mass density shifts positions of the extrema in comparison with analytical solution. This is one of the consequences of applying numerical solution by integrating number conservation law (for discussion see sec. 3.2).
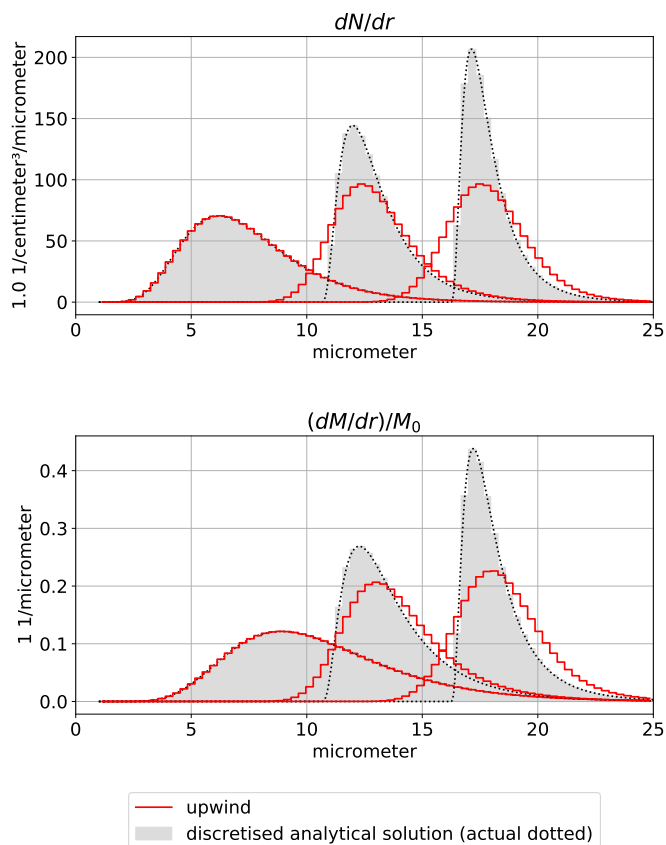
Figure 2. As in Fig. 1 for $p = r$ and $x = r$.

As can be seen in both the number- and mass-density plots in Figs. 1 and 2, solutions obtained with the upwind scheme are characterized by significant drop in the peak value and spectral broadening, with respect to the analytical solution – both manifesting the numerical diffusion.

The broadening and the drop in the peak value is less pronounced in Fig. 2 where the linear grid increases the resolution in the large-particle region of the spectrum.

2 MPDATA

2.1 Truncation error analysis of the upwind scheme

One of the methods used to quantify the numerical diffusion of the upwind scheme is the modified equation analysis of Hirt (1968) (see Margolin and Shashkov, 2006, for discussion in the context of MPDATA). To depict the idea, a simplified setting of $G = 1$ and $C = \mathrm{const}$ is outlined herein. In the analysis, the Taylor expansion of ψ up to the second order is taken at ψ_i^{n+1},

ψ_{i+1}^n and ψ_{i-1}^n and substituted into the numerical upwind scheme, in which the flux function (1.4) is expressed using moduli (e.g., Crowley, 1968, eq. (12)):

$$200 \quad \psi_i^{n+1} = \psi_i^n - \left(\frac{C + |C|}{2} (\psi_i^n - \psi_{i-1}^n) + \right.$$
$$\left. \frac{C - |C|}{2} (\psi_{i+1}^n - \psi_i^n) \right) \tag{2.1}$$

resulting in:

$$\partial_t \psi + \partial_t^2 \psi \frac{\Delta t}{2} = -\frac{u + |u|}{2} \left(\partial_x \psi - \partial_x^2 \psi \frac{\Delta x}{2} \right) -$$
$$\frac{u - |u|}{2} \left(\partial_x \psi + \partial_x^2 \psi \frac{\Delta x}{2} \right) \tag{2.2}$$

205   which is further transformed by employing a time derivative of both sides of the original advection equation $\partial_t \psi = -u \partial_x \psi \longrightarrow$ $\partial_t^2 \psi = -u \partial_x \partial_t \psi = u^2 \partial_x^2 \psi$ to substitute the second-order time derivative with spatial derivative (Cauchy-Kowalevski procedure, see Toro, 1999) leading to the sought modified equation (Roberts and Weiss, 1966, eq. 2.9):

$$\partial_t \psi + u \partial_x \psi + \underbrace{\left(u^2 \frac{\Delta t}{2} - |u| \frac{\Delta x}{2} \right)}_{K} \partial_x^2 \psi + ... = 0 \tag{2.3}$$

The above analysis depicts that the employment of the numerical scheme (1.3) results in a solution of a modified equation
210   (2.3), approximating the original problem up to first order. The leading second-order error contribution has the form of a diffusive term with a coefficient K (note that the above outline of the modified equation analysis assumes the constant velocity field). The diffusive form of the leading error term explains with the smoothing of the spectrum evident in Figs. 1,2, and hence the notion of numerical diffusion.

2.2   Antidiffusive velocity and iterative corrections

215   The problem of numerical diffusion can be addressed by introducing the so called "antidiffusive velocity" (Smolarkiewicz, 1983). To this end, the Fickian flux can be cast in the form of the advective flux - an approach dubbed pseudo-velocity technique in the context of advection-diffusion simulations (Lange, 1973, 1978) or hyperbolic formulation of diffusion (Cristiani, 2015, discussion of eq. (4) therein), and discussed in detail in Smolarkiewicz and Clark (1986, sect. 3.2):

$$\partial_x (K \partial_x \psi) = \partial_x \left(K \frac{\partial_x \psi}{\psi} \psi \right). \tag{2.4}$$

220   In Smolarkiewicz (1983, 1984), it was proposed to apply the identity (2.4) to equation (2.3) in order to suppress the spurious diffusion. The procedure is iterative. The first iteration is the basic upwind pass. Subsequent corrective iterations reverse the effect of numerical diffusion by performing upwind passes with the so-called antidiffusive flux based on equation (2.4) but with K taken with negative sign and approximated using the upwind stencil (for discussion of the discretization, see Smolarkiewicz and Margolin (2001)).
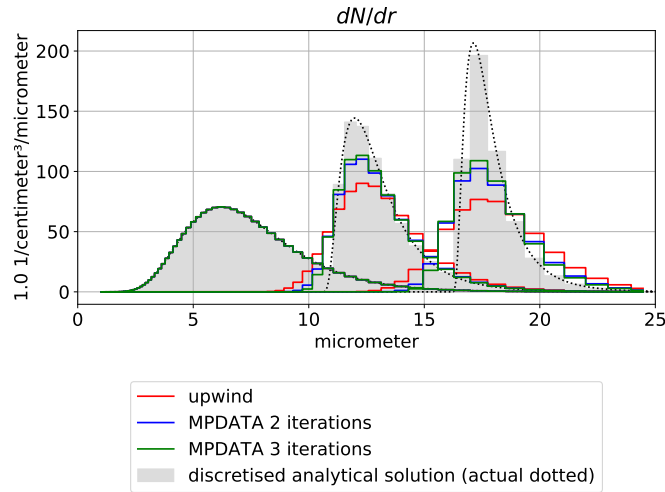
Figure 3. Comparison of analytic, upwind and MPDATA solutions (see plot key for algorithm variant specification) using the setup from Fig. 1, see sec. 2.2 for discussion.

Accordingly, the basic antidiffusive field $GC^{(k)}$ is defined as follows (with $\epsilon > 0$ being an arbitrary small constant used to prevent from divisions by zero):

$$GC_{i+\frac{1}{2}}^{(k)} = A_{i+\frac{1}{2}} \left(\left| GC_{i+\frac{1}{2}}^{(k-1)} \right| - \left(GC_{i+\frac{1}{2}}^{(k-1)} \right)^2 \right), \tag{2.5}$$

where k is the iteration number, $GC^{(1)} \equiv GC$ and

$$A_{i+\frac{1}{2}} = \frac{\psi_{i+1}^* - \psi_i^*}{\psi_{i+1}^* + \psi_i^* + \epsilon}, \tag{2.6}$$

where ψ^* denotes ψ^n in the first iteration, or the values resultant from application of the upwind scheme with the antidiffusive flux in subsequent iterations. The MPDATA scheme inherits the key properties of upwind in terms of positive-definiteness, conservativeness and stability, while reducing the effect of numerical diffusion. Given the context of conservation of particle concentration, in all presented numerical formulæ below, it is assumed that the transported signal is positive, the references provided include formulation of the algorithm for variable sign signals.

Figure 3 compares a set of example simulations performed with the same set-up as in Figure 1. The analytical results obtained with upwind are supplemented with results obtained using MPDATA scheme with two and three iterations. Employment of the MPDATA iteration corrects both the signal peak amplitude and its width, as well as the position of the maximum. It is visible that the effect of the third iteration is less pronounced than that of the second one. Overall, while the MPDATA solutions are superior to upwind, the drop in amplitude and broadening of the resultant spectrum still visibly differs from the discretized analytical solution.
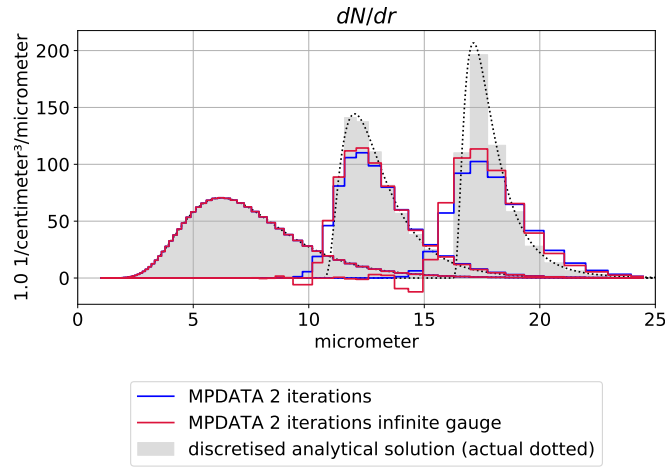
Figure 4. Comparison of analytic, upwind and MPDATA solutions (see plot key for algorithm variant specification) using the setup from Fig. 1, see sec. 2.3 for discussion.

2.3 Infinite gauge variant

For the possible improvement of the algorithm, one may consider linearizing MPDATA about an arbitrarily large constant (i.e. taking $\psi' = \psi + a\chi$ in the limit $a \longrightarrow \infty$ instead of ψ, where χ is a constant scalar background field). Such analysis was considered in Smolarkiewicz and Clark (1986, eq. 41) and subsequently referred to as the "infinite-gauge" (or "iga") variant of

245 MPDATA (Smolarkiewicz (2006, eq. 34), Margolin and Shashkov (2006, point (6) on page 1204)).

Such gauge transformation changes the corrective iterations of the basic algorithm as follows (replacing eqs. (2.6) and (1.4) what is symbolized with $\rightsquigarrow$):

$$A_{i+\frac{1}{2}} \quad \rightsquigarrow \quad A_{i+\frac{1}{2}}^{(\text{iga})} = \frac{\psi_{i+1}^* - \psi_i^*}{2} \tag{2.7}$$

$$F_{i+\frac{1}{2}} \quad \rightsquigarrow \quad F_{i+\frac{1}{2}}^{(\text{iga})} = GC_{i+\frac{1}{2}}^{(k)} \tag{2.8}$$

250 Noting that the amplitude of the diffusive flux (2.4) is inversely proportional to the amplitude of the signal, such gauge choice decreases the amplitude of the truncation error (see Smolarkiewicz and Clark (1986, p. 408), Jaruga et al. (2015, discussion of Fig. 11)), however it makes the algorithm no longer positive definite.

Figure 4 depicts how enabling the infinite gauge variant influences results presented in Figure 3. In each plotted time step, the maximum amplitude of the infinite-gauge result is closest to the analytical solution improving over the basic MPDATA.

255 However, in each case negative values are observed (non-physical in case of the considered problem).

Consequently, for the problem at hand, it is effectively essential to combine it with the monotonicity-preserving non-oscillatory option outlined in the next section.

2.4 Non-oscillatory option

In Smolarkiewicz and Grabowski (1990), extension of the MPDATA algorithm was introduced that makes the solution mono-
260 tonicity preserving and precludes appearance of negative values in the discussed solution of droplet size spectrum evolution.
The trade-off is that the order of the algorithm is reduced (see Appendix A).

The non-oscillatory option (later referred to as "non-osc" herein) modifies the algorithm in such way:

$$
GC^{(k+1)}_{i+\frac{1}{2}} \rightsquigarrow GC^{(k+1,\text{non-osc})}_{i+\frac{1}{2}} = GC^{(k)}_{i+\frac{1}{2}} \times
$$

$$
\times
\begin{cases}
\min(1, \beta_i^\downarrow, \beta_{i+1}^\uparrow) & GC^{(k)}_{i+\frac{1}{2}} \geq 0 \\
\min(1, \beta_i^\uparrow, \beta_{i+1}^\downarrow) & GC^{(k)}_{i+\frac{1}{2}} < 0
\end{cases},
\tag{2.9}
$$

265 where

$$
\beta_i^\uparrow \equiv G_i \times \frac{\max\left(\psi_i^{(\text{max})}, \psi_{i-1}^*, \psi_i^*, \psi_{i+1}^*\right) - \psi_i^*}{\max\left(F(\psi^*)_{i-\frac{1}{2}}, 0\right) - \min\left(F(\psi_i^*)_{i+\frac{1}{2}}, 0\right) + \epsilon},
\tag{2.10}
$$

and

$$
\beta_i^\downarrow \equiv G_i \times \frac{\min\left(\psi_i^{(\text{min})}, \psi_{i-1}^*, \psi_i^*, \psi_{i+1}^*\right) - \psi_i^*}{\max\left(F(\psi_i^*)_{i+\frac{1}{2}}, 0\right) - \min\left(F(\psi_i^*)_{i-\frac{1}{2}}, 0\right) + \epsilon},
\tag{2.11}
$$

with

$$
270 \quad \psi_i^{(\text{min})} = \min(\psi_{i-1}^n, \psi_i^n, \psi_{i+1}^n),
\tag{2.12}
$$

$$
\psi_i^{(\text{max})} = \max(\psi_{i-1}^n, \psi_i^n, \psi_{i+1}^n).
\tag{2.13}
$$

Note that in the case of infinite gauge option enabled, F function takes form presented in eq. (2.7) (see also Hill, 2011, sect. 2.5).

Figure 5 juxtaposes infinite gauge solutions for non-oscillatory option switched on or off. The effectiveness of the latter
variant is apparent as spurious negative values no longer occur.

275 ## 2.5 DPDC

An alternative approach to the iterative procedure was introduced in Beason and Margolin (1988); Margolin and Smolarkiewicz
(1998) and further discussed in Margolin and Shashkov (2006), where the contributions of multiple corrective iterations of
MPDATA were analytically summed leading to a new two-pass scheme dubbed DPDC (double-pass donor cell), featuring the
following form of the antidiffusive GC field:

$$
280 \quad GC^{(2)}_{i+\frac{1}{2}} \rightsquigarrow GC^{(\text{DPDC})}_{i+\frac{1}{2}} = \frac{GC^{(2)}}{1 - |A_{i+\frac{1}{2}}|} \left(1 - \frac{GC^{(2)}}{1 - A^2_{i+\frac{1}{2}}}\right),
\tag{2.14}
$$

with $A_{i+\frac{1}{2}}$ defined in eq. (2.6). Note that only one corrective iteration is performed with the DPDC variant.

As in the case of the infinite gauge variant of MPDATA (section 2.3), the above formulation does not guarantee monotonicity
of the solution. Herein an example simulation combining the DPDC, the non-oscillatory and infinite-gauge variants is presented
in Figure 6 depicting how the solution is improved over that in Figure 5.
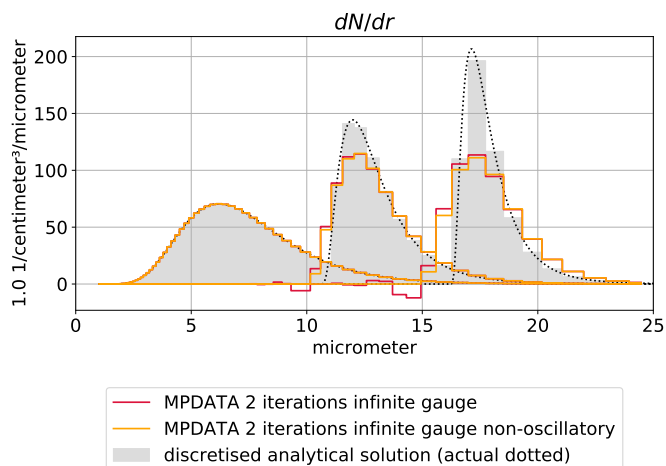
Figure 5. Comparison of analytic, upwind and MPDATA solutions (see plot key for algorithm variant specification) using the setup from Fig. 1, see sec. 2.4 for discussion.
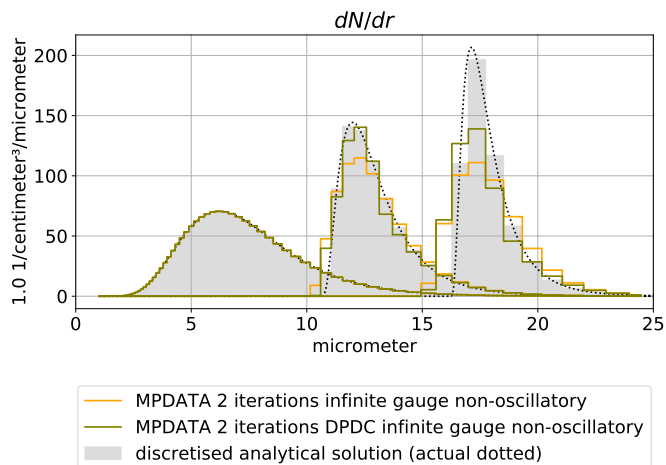
Figure 6. Comparison of analytic, upwind and MPDATA solutions (see plot key for algorithm variant specification) using the setup from Fig. 1, see sec. 2.5 for discussion.

2.6 Divergent-flow correction

For divergent flow (hereinafter abbreviated dfl), modified equation analysis yields an additional correction term to the antidiffusive velocity (see Smolarkiewicz (1984, eq. (38)) for uniform coordinates, Margolin and Smolarkiewicz (1998, eq. (30)) for non-uniform coordinates and Waruszewski et al. (2018, sect. 4) for the infinite-gauge variant):

$$
GC^{(k)}_{i+\frac{1}{2}} \rightsquigarrow GC^{(\text{k,dfl})}_{i+\frac{1}{2}} = GC^{(k)} - \frac{GC^{(k)}_{i+\frac{1}{2}}}{G_{i+1}+G_i} \times
$$

290
$$
\times \frac{GC^{(k)}_{i+\frac{3}{2}} - GC^{(k)}_{i-1/2}}{2} \times
$$

$$
\times \begin{cases} (\psi^*_{i+1} + \psi^*_i)/2 & (iga) \\ 1 & (else) \end{cases} \tag{2.15}
$$

As pointed out in section 5.1 in Smolarkiewicz (1984), this option has the potential of improving results for the problem of the evolution of the droplet size distribution (personal communication with William Hall cited therein). This is due to the drop growth velocity defined by eq. (1.5) being dependent on radius (hence divergent given the one-dimensional problem). Yet,

295 applying adequate coordinate transformation (i.e., $p = r^2$), the drop growth velocity in the transformed coordinates becomes constant (see section 1.5 above and Hall (see, e.g. 1980, sec. 3b)). However, in simulations using the presented setup (for $p \neq r^2$; not shown), only insignificant changes in the signal occurring when the divergent-flow option was used were observed. However, the problem considered herein does not include, for instance, the surface tension influence on the drop growth rate.

2.7 Third order terms

300 Another possible improvement to the algorithm comes from the inclusion of the third-order terms in the modified equation analysis, which leads to following form of the antidiffusive velocity (Margolin and Smolarkiewicz, 1998):

$$
GC^{(k)}_{i+\frac{1}{2}} \rightsquigarrow GC^{(\text{k,tot})}_{i+\frac{1}{2}} = GC^{(k)} + B_i \cdot GC^{(k)}_{i+\frac{1}{2}} \times
$$

$$
\times \frac{1}{6}\left(4\frac{|GC^{(k)}_{i+\frac{1}{2}}|}{G_{i+1}+G_i} - 8\left(\frac{GC^{(k)}_{i+\frac{1}{2}}}{G_{i+1}+G_i}\right)^2 - 1\right) \tag{2.16}
$$

$$
B_i = 2 \cdot (\psi^*_{i+2} - \psi^*_{i+1} - \psi^*_i + \psi^*_{i-1}) \times
$$

305
$$
\times \begin{cases} (1+1+1+1)^{-1} & (iga) \\ (\psi^*_{i+2} + \psi^*_{i+1} + \psi^*_i + \psi^*_{i-1})^{-1} & (else) \end{cases} \tag{2.17}
$$

Figure 7 depicts how enabling the third-order-terms improves solution of the test problem with respect to the upwind and basic MPDATA.

Noteworthy, discussion of higher-order variants of MPDATA was carried forward in Kuo et al. (1999) and Waruszewski et al. (2018). In the latter case, the focus was placed on accounting for coordinate transformation and variable velocity in the

310 derivation of antidiffusive velocities leading to a fully third-order accurate scheme.
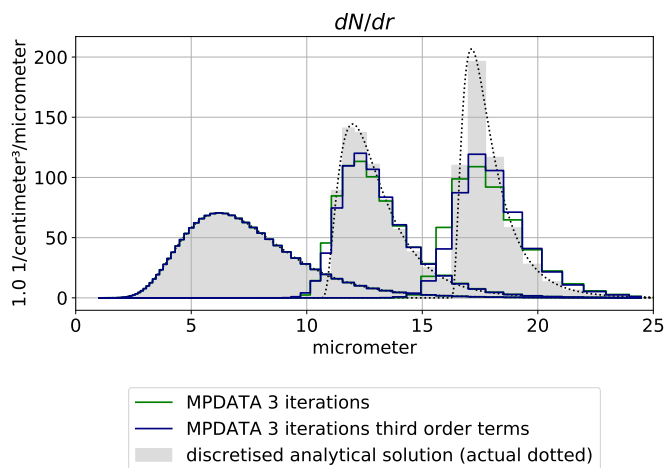
Figure 7. Comparison of analytic, upwind and MPDATA solutions (see plot key for algorithm variant specification) using the setup from Fig. 1, see sec. 2.7 for discussion.
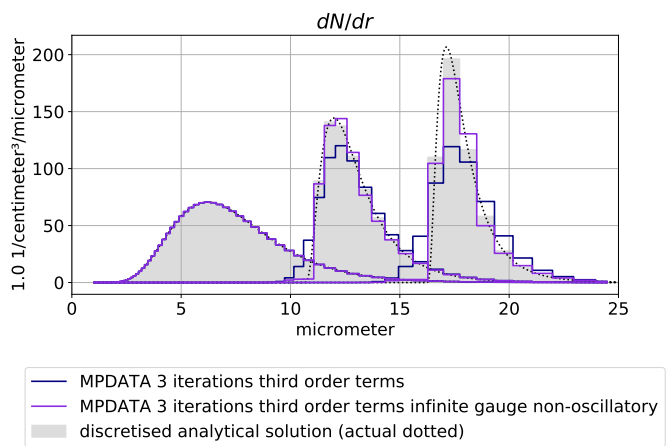
Figure 8. Comparison of analytic, upwind and MPDATA solutions (see plot key for algorithm variant specification) using the setup from Fig. 1, see sec. 2.8 for discussion.

2.8 A "best" combination of options

The MPDATA variants presented in the preceding sections can be combined together. In Figure 8, results obtained with upwind scheme and the basic two-pass MPDATA are compared with those obtained with a powerful combination of three iterations, third-order-terms, infinite-gauge and non-oscillatory options hereinafter referred to as the "best" variant (for the problem at 315 hand).

Table 1. Relative dispersion of the discretized (using grid setup as in Fig. 1) analytical solution taken for five selected times.

Variant	d_{analytic}
$d(M = 1 \, \text{g} \, \text{kg}^{-1})$	0.357
$d(M = 2 \, \text{g} \, \text{kg}^{-1})$	0.202
$d(M = 4 \, \text{g} \, \text{kg}^{-1})$	0.126
$d(M = 6 \, \text{g} \, \text{kg}^{-1})$	0.097
$d(M = 8 \, \text{g} \, \text{kg}^{-1})$	0.080
$d(M = 10 \, \text{g} \, \text{kg}^{-1})$	0.069

3 Results and discussion

In the following subsections, the influence of MPDATA algorithm variant choice on the resultant spectrum broadness and computational cost is analysed using the example simulation setup used above (i.e., in all figures except Fig. 2, see section 1.5 for test case definition).

320   Analysis of the scheme solution convergence with changing resolution and Courant number is presented in Appendix A.

3.1 Quantification of numerical broadening

The relative dispersion, defined as the ratio of standard deviation σ to the mean μ of the distribution, is a parameter commonly used to describe the width of the spectrum (e.g. Chandrakar et al., 2018).

     The calculated dispersion ratio over all bins takes form:

$$325 \quad d = \frac{\sqrt{\frac{1}{N} \sum_i m_i^{(l=2)} - \left(\frac{1}{N} \sum_i m_i^{(l=1)} \right)^2}}{\frac{1}{N} \sum_i m_i^{(l=1)}} \tag{3.1}$$

where m_i is defined in (1.8) and N is the conserved total number of particles (equal to $\sum_i m_i^{(l=0)}$). To quantify the effect of numerical diffusion on the broadness of the resultant spectrum, the following parameter is introduced based on the numerical and analytical solutions (hereinafter reported in percentages):

$$R_{\text{disp}} = d_{\text{numerical}} / d_{\text{analytical}} - 1 \tag{3.2}$$

330   Table 1 depicts the gradual narrowing of the spectrum under undisturbed adiabatic growth.

     Left panel in Fig. 9 provides values of the R_{disp} parameter evaluated at six selected timesteps corresponding to $M = 1, 2, 4, 6, 8, 10 \, \text{g} \, \text{kg}^{-1}$. Although numerical broadening is inherent to all employed schemes, and grows in time for all considered variants, the scale of the effect is significantly reduced when using MPDATA.

     In particular, a tenfold decrease in numerical broadening as quantified using R_{disp} is observed comparing upwind and "best"
335   variant considered herein.

While outside of the scope of the present study, it is worth noting that in simulations combining spectral growth with transport in physical space, the numerical broadening associated with the spatial advection also contributes to the numerical broadening effect (see Pardo et al., 2020, and references therein).

3.2 Notes on conservativeness

340 Due to the formulation of the problem as number conservation and discretization of the evolution equation using fixed bins, even though the numerical scheme is conservative (up to subtle limitations outlined below), evaluation of other statistical moments of the evolved distribution from the number density introduces an inherent discrepancy from the analytical results (for a discussion on multi-moment formulation of the problem, see e.g. Liu et al., 1997).

In order to quantify the discrepancy in the total mass between the discretized analytical solution and the numerically inte-
345 grated spectrum, the following ratio is defined using moment evaluation formula (1.8):

$$R_M = M^{(\text{numeric})}/M^{(\text{analytic})} - 1 =$$
$$= \frac{\sum_i m_i^{(l=3,\,\text{numeric})}}{\sum_i m_i^{(l=3,\,\text{analytic})}} - 1. \tag{3.3}$$

Right panel in Fig. 9 depicts the values of the above-defined ratio computed for spectra obtained with different variants of MPDATA discussed herein. The departures from analytically-derived values are largest for the upwind scheme (up to ca. 5%),
350 and oscillate around 0 with amplitude of the order of 1% for most of the MPDATA solutions.

The consequences of mass conservation inaccuracies in the fixed-bin particle size spectrum representation may not be as severe as in, e.g. dynamical core responsible for transport of conserved scalar fields. The outlined discrepancies may be dealt with by calculating the change in mass during a time step from condensation, then using it in vapor and latent heat budget calculations so the total mass and energy in the modeled system are conserved.

355 The problem embodied in equation (1.1) is the conservation of number of particles and the embraced algorithm (1.3)-(1.4) is conservative (up to numerical precision) for $G = 1$. However, the formulation of the donor cell scheme $\psi^{n+1} = \psi^n + G_i^{-1}\left(F_{i-1/2} + F_{i+\frac{1}{2}}\right)$ on the staggered grid with $G \neq 1$, for example due to employment of non-identity coordinate transformations implies that even though the influx and outflux across boundary of adjacent cells is equal, discretization of G_i at cell centers limits the level of accuracy in number conservation.

360 The total number of particles in the system may diverge from the analytical expected value even for the initial condition depending on the employed discretization approach. In the present work, the probability density function is probed at cell centers effectively assuming piecewise-constant number density function. An alternative approach is to discretise the initial probabilities by assigning to ψ_i the values of $(\phi_{i+\frac{1}{2}} - \phi_{i-1/2})/(r_{i+\frac{1}{2}} - r_{i-1/2})$ where ϕ is the cumulative distribution.

3.3 Computational cost

365 Table 2 includes an assessment of the relative computational cost of the explored variants of MPDATA. The performance was estimated by repeated measurements of the wall time and selecting the minimal value as representative. Values are reported
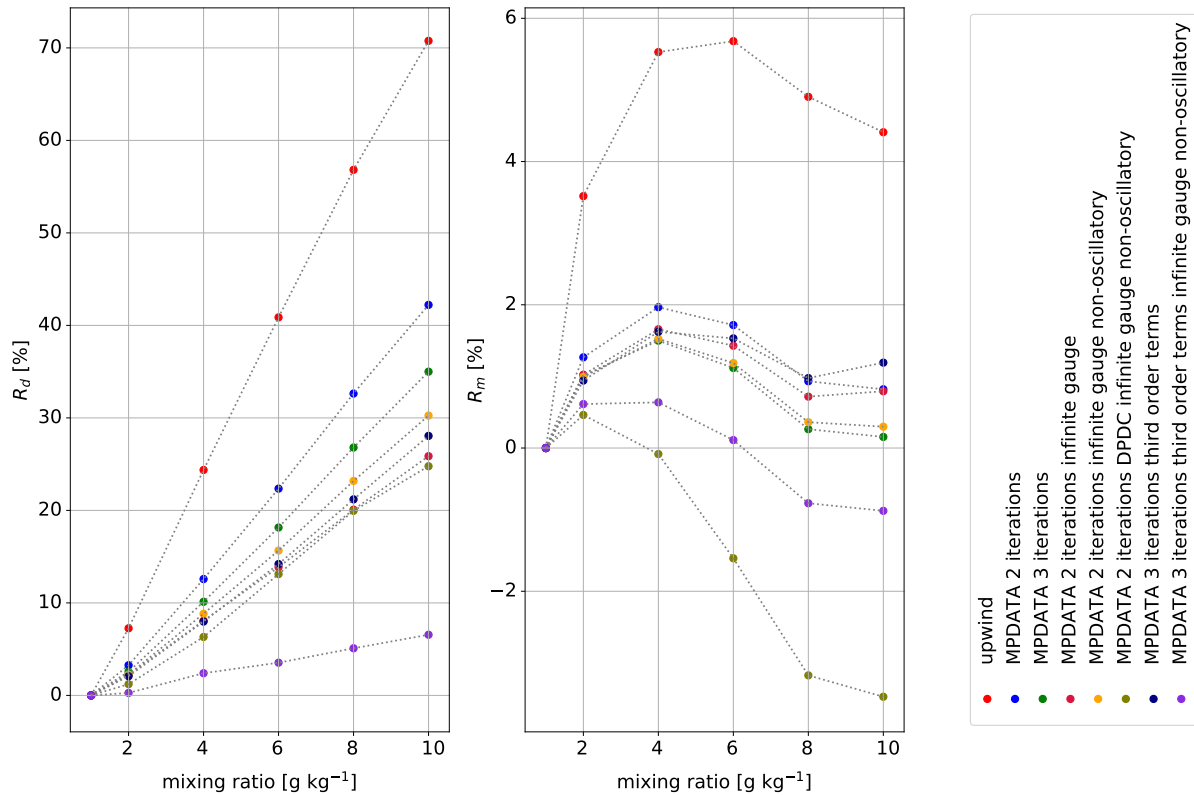
Figure 9. Left panel summarizes values of R_d (see eq. (3.2) for definition) computed for simulations using different discussed variants of MPDATA and plotted as a function of increasing mixing ratio (i.e., each simulation is depicted with a set of line-connected points corresponding to selected timesteps), see section 3.1. Right panel presents analogous analysis for R_m, see section 3.2 for discussion. Note: $R_M = R_d = 0$ corresponds to perfect match with the analytical solution.)

after normalization with respect to the values pertinent to upwind runs. The "best" variant is roughly ten times more costly than the upwind scheme. The table includes analogous measurements reported in earlier studies on MPDATA, where available (see Table caption for comments).

370   As can be seen from the table, the infinite gauge option not only improves result, but simplifies equation, making numerics faster. Three-pass MPDATA with third order terms included is slightly faster than the variant with both the infinite-gauge and non-oscillatory options enabled.

Although the discussed problem is one-dimensional, its computationally efficient and accurate solution is essential, as it typically needs to be solved at every time step and grid point of a three-dimensional cloud model.

Table 2. Elapsed wall times with respect to upwind computed for mass doubling grid for results presented herein compared with with data reported in three previously published works. Column labeled with S83 denotes values reported in Smolarkiewicz (1983) for two-dimensional problem. Column labeled SS05 correspond to data reported in Smolarkiewicz and Szmelter (2005) for a 3D finite-volume advection on unstructured grid. Column SR91 includes values from Smolarkiewicz and Rasch (1991), MSS00 corresponds to data from Margolin et al. (2000), both reported for two-dimensional problems.

Variant		S83	SS05	SR91	MSS00
upwind	1.0	1.0	1.0	1.0	1.0
2 pass	2.5	2.9	4.3	5.4	3.7
2 pass, iga	2.2	-	1.9	-	-
2 pass, iga, non-osc	5.9	-	3.9	-	-
DPDC, iga, non-osc	6.2	-	-	-	-
3 pass	5.7	5	-	9.8	-
3 pass, tot	4.1	-	-	19	-
3 pass, tot, iga, non-osc	11	-	-	-	-

375 4   Conclusions

The study was focused on the MPDATA family of numerical schemes that iteratively apply the upwind algorithm reducing the numerical diffusion while maintaining the salient features of the underlying upwind scheme such as conservativeness and positive-definiteness.

Several options introduced to MPDATA following its original formulation were explored here in the context of condensa-
380 tional growth problems. This included the procedure to introduce coordinate transformations (e.g., to a mass-doubling grid) and the variants of MPDATA including: infinite-gauge, non-oscillatory, DPDC and third-order-terms options.

In literature, the derivation and discussion of MPDATA variants is spread across numerous research papers published across almost four decades, and in most cases focused on multidimensional hydrodynamics applications. It seems that this contributed to an apparent detachment of condensational-growth applications from the benefits of continuous research on MPDATA. It was
385 the aim of this study, to highlight the developments that followed the original formulation of the algorithm, and to highlight their applicability to the problem. To this end, it was shown that combination of such features of MPDATA as the infinite-gauge, non-oscillatory and third-order-terms options, together with application of multiple corrective iterations offer a robust scheme that grossly outperforms the almost quadragenarian basic MPDATA.

Code availability. All of presented figures and tables can be recreated in interactive notebooks "in the cloud" using the mybinder.org or

390 Colab platforms. To launch the notebooks, follow the link:

https://github.com/atmos-cloud-sim-uj/PyMPDATA/tree/master/PyMPDATA_examples/Olesik_et_al_2020.

The calculations are performed using newly developed open-source Pythonic implementation of MPDATA: PyMPDATA (Arabas et al., 2020). In terms of numerics, implementation of PyMPDATA closely follows libmpdata++ (Jaruga et al., 2015).

The electronic supplement to this manuscript contains a snapshot of the project code repository archived at the day of submission. The 1.0

395 release stated in the title is going to accompany the final version of the article.

PyMPDATA development is hosted at: https://github.com/atmos-cloud-sim-uj/PyMPDATA. PyMPDATA is licenced under the GNU General Public License 3.0.

Appendix A: Convergence analysis

To assess the spatial and temporal convergence of the numerical solutions presented above, a convergence test originating

400 from Smolarkiewicz and Grabowski (1990) is used. For the analysis the following truncation-error L^2 measure is used (e.g., Smolarkiewicz, 1984):

$$\text{Err}_{L2} = \frac{1}{T}\sqrt{\sum_i \left(\psi_i^{\text{numerical}} - \psi_i^{\text{analytical}}\right)^2 / nx}. \tag{A1}$$

As a side note, it is worth pointing out that for the chosen coordinates $\left(p = r^2, x = r^2\right)$, the coordinate transformation term is equal to identity, so there is no need for including the G factor into the computed error measures. In general case, convergence

405 will depend on the grid choice and to account for that one may used a modified measure as given in Smolarkiewicz and Rasch (1991, eq. 24).

To explore the convergence, the error measures are computed for 7 different linearly spaced values of C between 0.05 and .95, and $nx \in \left\{2^7, 2^8, 2^9, 2^{10}, 2^{11}, 2^{12}, 2^{13}, 2^{14}\right\}$ resulting in 56 simulations for each presented combination of options.

As proposed in Smolarkiewicz and Grabowski (1990), visualization of the results is carried out on polar plots with radius ρ

410 and angle ϕ coordinates defined as follows:

$$\rho = \ln_2\left(\frac{1}{nx}\right) + \text{const}, \quad \phi = C\frac{\pi}{2}, \tag{A2}$$

where ρ was shifted by a constant so that the highest resolution grid corresponds to $\rho = 1$.

Figures A1-A8 depict the convergence rates and are intended for comparison with analogously constructed plots in Figs. 2-3 Smolarkiewicz and Grabowski (1990), Figs. 8.1-8.2 Margolin and Smolarkiewicz (1998) and Figs. 10-11 Jaruga et al. (2015).

415 The chosen color increments correspond to the error reduction by a factor of 2, the warmer the color, the larger the error. The small gray points behind the isolines represent points for which the error value was calculated. When moving along the lines of constant Courant number, increasing the space and time discretization, number of crossed dashed isolines indicate the order of convergence. For the considered problem, it can be seen that the upwind scheme (Fig. A1) has convergence of the first order (one isoline is crossed when spatial discretization increases by one order); MPDATA scheme (Fig. A2) of the second order and

420 MPDATA with 3 iterations (Fig. A6) is of the third order.
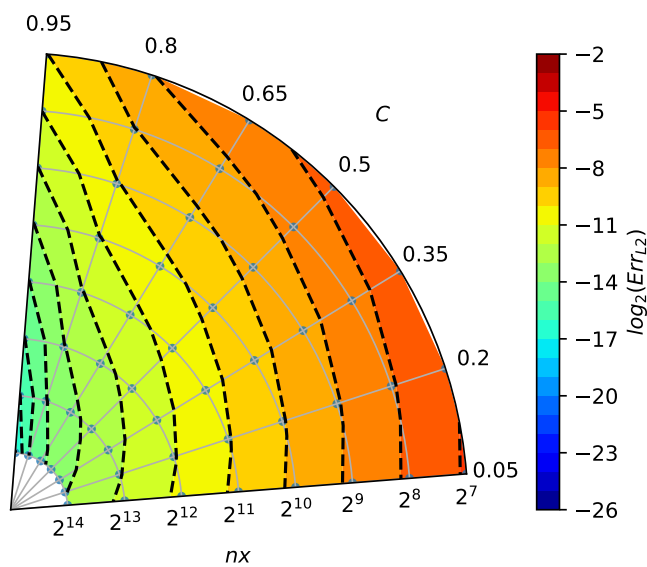
Figure A1. Convergence plot for the upwind scheme (cf. Fig. 1)
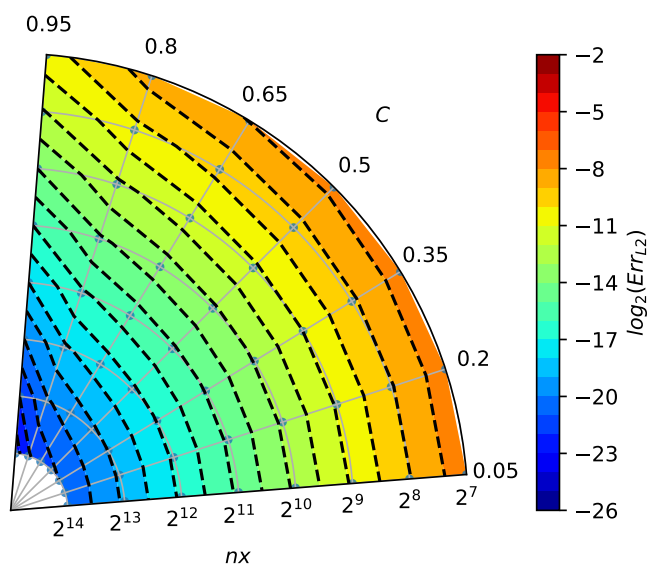
Figure A2. Convergence plot for basic 2-pass MPDATA (cf. Fig. 3)
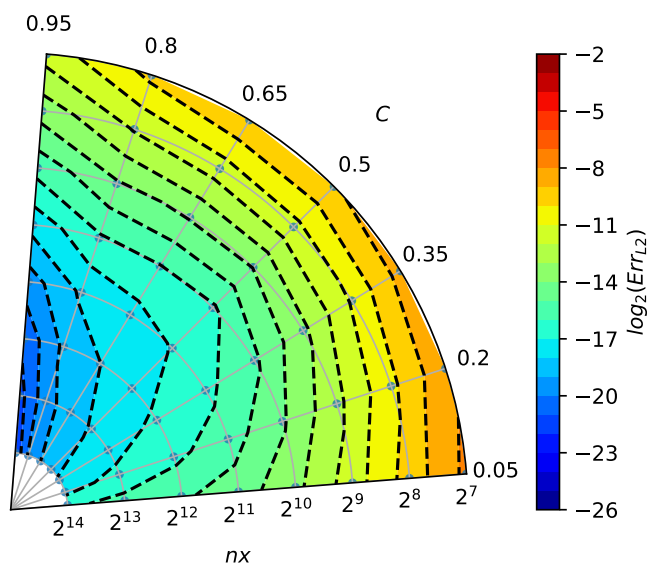
Figure A3. Convergence plot for the infinite gauge MPDATA (cf. Fig. 4)
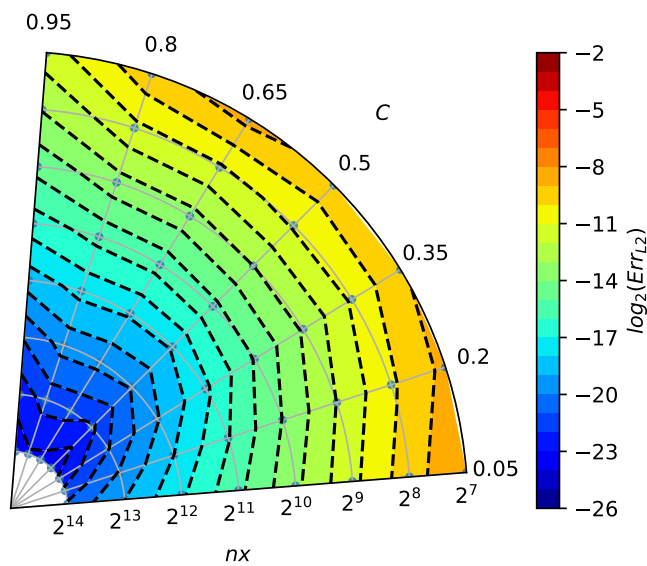
Figure A4. Convergence plot for the infinite gauge non-oscillatory variant of MPDATA (cf. Fig. 5)
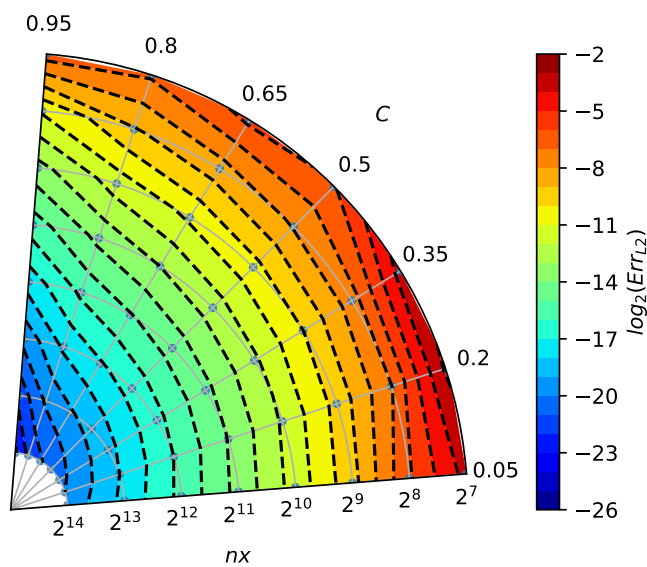
Figure A5. Convergence plot for the DPDC variant with infinite gauge and non-oscillatory corrections (cf. Fig. 6)
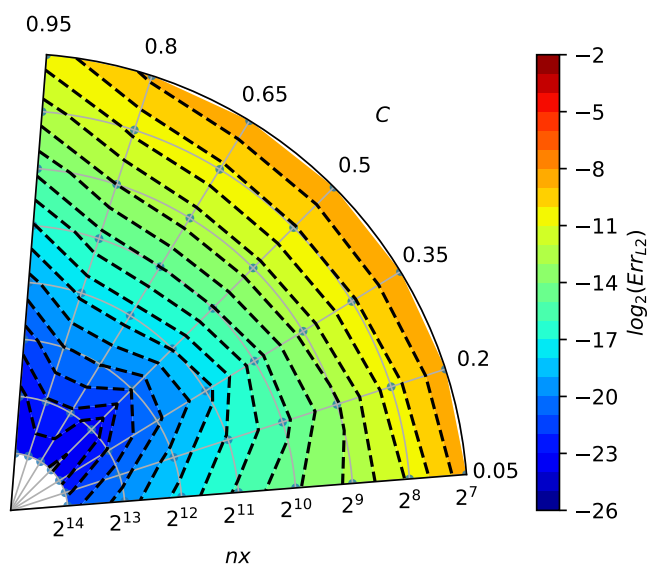
Figure A6. Convergence plot for the three-pass MPDATA (cf. Fig. 3)
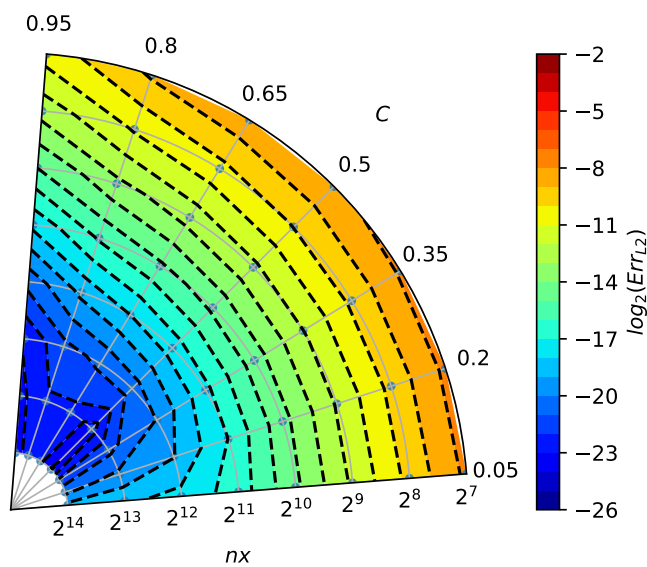
Figure A7. Convergence plot for the three-pass MPDATA with third order terms (cf. Fig. 7)
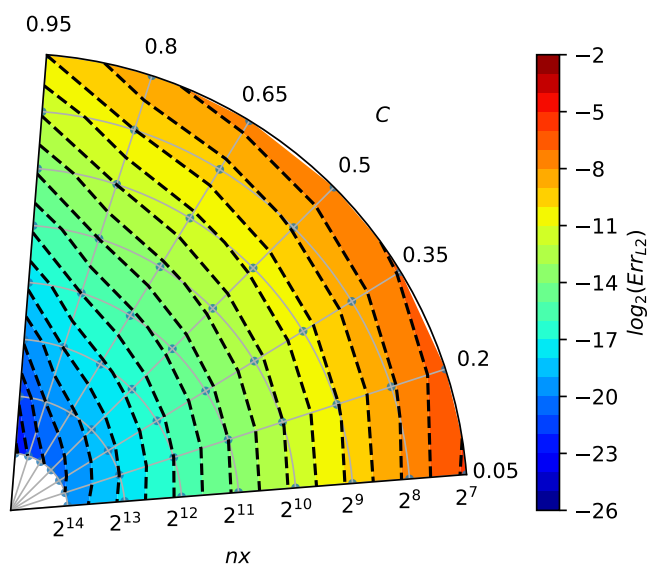
Figure A8. Convergence plot for the three-pass infinite gauge non-oscillatory MPDATA with third order term corrections (cf. Fig. 8).

Moreover, the shape of the dashed isolines tells the dependency of the solution accuracy on the Courant number. When these are isotropic (truncation error being independent of polar angle), the solution is independent of the Courant number.

An interesting behavior of the schemes can be seen for Fig. A3 and Fig. A4, where the groove of the third-order convergence rate forms around $\phi = \frac{\pi}{4}$, normally characteristic for MPDATA with three or more passes. When second-order truncation error

425 is sufficiently reduced, the third-order error, proportional to $(1 - 3C + 2C^2)$ as can be seen in (2.16), dominates, but vanishes for $C = 0.5$, thus resulting in the existence of the groove.

The convergence test result for the three-pass MPDATA with infinite gauge, non-oscillatory and third order terms options enabled (Fig. A8) are consistend with results depicted in Fig. A7, although the order of convergence is reduced due to the employment of non-oscillatory option.

430 *Author contributions.* The idea of the study originated in discussions between SA, SU and MO. MO led the work and preliminary version of significant part of the presented material constituted his MSc thesis prepared under mentorship of SA. PB architected the key components of PyMPDATA package. JB contributed the DPDC variant of MPDATA to PyMPDATA. MB participated in composing the paper and devising result analysis workflow. All authors contributed to the final form of the text.

Competing interests. The authors declare no competing interests.

435 *Acknowledgements.* The manuscript and the developed code benefited from comments and contributions from (in alphabetical order): Szymon Drenda, Wojciech Grabowski, Hugh Morrison, Andrzej Odrzywołek, Piotr Smolarkiewicz and Maciej Waruszewski. The project was carried out with support from the Foundation for Polish Science (POIR.04.04.00-00-5E1C/18-00).

References

Abade, G., Grabowski, W. W., and Pawlowska, H.: Broadening of Cloud Droplet Spectra through Eddy Hopping: Turbulent Entraining Parcel
440   Simulations, J. Atmos. Sci., 75, https://doi.org/10.1175/JAS-D-18-0078.1, 2018.

Arabas, S. and Pawlowska, H.: Adaptive method of lines for multi-component aerosol condensational growth and CCN activation, Geosci.
Model Dev., 4, https://doi.org/10.5194/gmd-4-15-2011, 2011.

Arabas, S. and Shima, S.: On the CCN (de)activation nonlinearities, Nonlin. Proc. Geophys., 24, https://doi.org/10.5194/npg-24-535-2017,
2017.

445   Arabas, S., Bartman, P., and Olesik, M.: https://github.com/atmos-cloud-sim-uj/PyMPDATA, 2020.

Beason, C. W. and Margolin, L. G.: DPDC (double-pass donor cell): A second-order monotone scheme for advection, in: Fifth Nuclear Code
Developers' Conference, https://www.osti.gov/servlets/purl/7049237, LLNL report UCRL-99731, 1988.

Brown, R.: A numerical study of radiation fog with an explicit formulation of the microphysics, Q. J. R. Meteorol. Soc., 106,
https://doi.org/10.1002/qj.49710645010, 1980.

450   Chandrakar, K. K., Cantrell, W., and Shaw, R. A.: Influence of Turbulent Fluctuations on Cloud Droplet Size Dispersion and Aerosol Indirect
Effects, J. Atmos. Sci., 75, https://doi.org/10.1175/JAS-D-18-0006.1, 2018.

Courant, R., Isaacson, E., and Rees, M.: On the solution of nonlinear hyperbolic differential equations by finite differences, Comm. Pure
Appl. Math, 5, https://doi.org/10.1002/cpa.3160050303, 1952.

Cristiani, E.: Blending Brownian motion and heat equation, J. Coupled Syst. Multiscale Dyn., 3, https://doi.org/10.1166/jcsmd.2015.1089,
455   2015.

Crowley, W. P.: Numerical Advection Experiments, Mon. Weather Rev., 96, https://doi.org/10.1175/1520-
0493(1968)096<0001:NAE>2.0.CO;2, 1968.

Devenish, B. J., Bartello, P., Brenguier, J.-L., Collins, L. R., Grabowski, W. W., IJzermans, R. H. A., Malinowski, S. P., Reeks,
M. W., Vassilicos, J. C., Wang, L.-P., and Warhaft, Z.: Droplet growth in warm turbulent clouds, Q. J. R. Meteorol. Soc., 138,
460   https://doi.org/10.1002/qj.1897, 2012.

Dhaniyala, S. and Wexler, A. S.: Numerical schemes to model condensation and evaporation of aerosols, Atmos. Env., 30,
https://doi.org/10.1016/1352-2310(95)00288-X, 1996.

East, T. W. R.: An inherent precipitation mechanism in cumulus clouds, Q. J. R. Meteorol. Soc., 83, https://doi.org/10.1002/qj.49708335506,
1957.

465   Grabowski, W. and Wang, L.-P.: Growth of Cloud Droplets in a Turbulent Environment, Annu. Rev. Fluid Mech., 45,
https://doi.org/10.1146/annurev-fluid-011212-140750, 2013.

Grabowski, W. W.: Comparison of Eulerian bin and Lagrangian particle-based microphysics in simulations of nonprecipitating cumulus, J.
Atmos. Sci., https://doi.org/10.1175/JAS-D-20-0100.1, 2020.

Grabowski, W. W., Morrison, H., Shima, S.-I., Abade, G. C., Dziekan, P., and Pawlowska, H.: Modeling of Cloud Microphysics: Can We Do
470   Better?, Bulletin of the American Meteorological Society, 100, https://doi.org/10.1175/BAMS-D-18-0005.1, 2019.

Hall, W. D.: A Detailed Microphysical Model Within a Two-Dimensional Dynamic Framework: Model Description and Preliminary Results,
J. Atmos. Sci, 37, https://doi.org/10.1175/1520-0469(1980)037<2486:ADMMWA>2.0.CO;2, 1980.

Hill, R. N.: Numerical modelling of multi-material interfaces, Ph.D. thesis, Loughborough University, https://hdl.handle.net/2134/8103,
2011.

475 Hirt, C. W.: Heuristic stability theory for finite-difference equations, J. Comput. Phys., https://doi.org/10.1016/0021-9991(68)90041-7, 1968.

Howell, W.: The growth of cloud drops in uniformly cooled air, J. Meteorol., 6, https://doi.org/10.1175/1520-0469(1949)006<0134:TGOCDI>2.0.CO;2, 1949.

Hulburt, H. and Katz, S.: Some problems in particle technology: A statistical mechanical formulation, Chem. Eng. Sci, 19, https://doi.org//10.1016/0009-2509(64)85047-8, 1964.

480 Jaruga, A., Arabas, S., Jarecka, D., Pawlowska, H., Smolarkiewicz, P. K., and Waruszewski, M.: libmpdata++ 1.0: a library of parallel MPDATA solvers for systems of generalised transport equations, Geosci. Model Dev., 8, https://doi.org/10.5194/gmd-8-1005-2015, 2015.

Jeffery, C. A., Reisner, J. M., and Andrejczuk, M.: Another Look at Stochastic Condensation for Subgrid Cloud Modeling: Adiabatic Evolution and Effects, J. Atmos. Sci., 64, https://doi.org/10.1175/2006JAS2147.1, 2007.

Khain, A. P., Beheng, K. D., Heymsfield, A., Korolev, A., Krichak, S. O., Levin, Z., Pinsky, M., Phillips, V., Prabhakaran, T., Teller, A.,
485 van den Heever, S. C., and Yano, J.-I.: Representation of microphysical processes in cloud-resolving models: Spectral (bin) microphysics versus bulk parameterization, Rev. Geophys., 53, https://doi.org/10.1002/2014RG000468, 2015.

Kostinski, A. B. and Jameson, A. R.: On the Spatial Distribution of Cloud Particles, J. Atmos. Sci., 57, https://doi.org/10.1175/1520-0469(2000)057<0901:OTSDOC>2.0.CO;2, 2000.

Kostoglou, M. and Karabelas, A. J.: Evaluation of Numerical Methods for Simulating an Evolving Particle Size Distribution in Growth
490 Processes, Chem. Eng. Comm., 136, https://doi.org/10.1080/00986449508936360, 1995.

Kovetz, A.: An Analytical Solution for the Change of Cloud and Fog Droplet Spectra Due to Condensation, J. Atmos. Sci, 26, https://doi.org/10.1175/1520-0469(1969)026<0302:AASFTC>2.0.CO;2, 1969.

Kovetz, A. and Olund, B.: The Effect of Coalescence and Condensation on Rain Formation in a Cloud of Finite Vertical Extent, J. Atmos. Sci, 26, https://doi.org/10.1175/1520-0469(1969)026<1060:TEOCAC>2.0.CO;2, 1969.

495 Kühnlein, C. and Smolarkiewicz, P. K.: An unstructured-mesh finite-volume MPDATA for compressible atmospheric dynamics, J. Comp. Phys., 334, https://doi.org/10.1016/j.jcp.2016.12.054, 2017.

Kuo, H.-C., Leou, T.-M., and Williams, R. T.: A study on the high-order Smolarkiewicz methods, Comput. Fluids, 28, https://doi.org/10.1016/s0045-7930(98)00036-x, 1999.

Lange, R.: ADPIC: a three-dimensional computer code for the study of pollutant dispersal and deposition under complex conditions,
500 https://doi.org/10.2172/4308175, LLNL report no. UCRL-51462, 1973.

Lange, R.: ADPIC—A Three-Dimensional Particle-in-Cell Model for the Dispersal of Atmospheric Pollutants and its Comparison to Regional Tracer Studies, J. Appl. Meteorol., 17, https://doi.org/10.1175/1520-0450(1978)017<0320:ATDPIC>2.0.CO;2, 1978.

Li, X.-Y., Brandenburg, A., Haugen, N. E. L., and Svensson, G.: Eulerian and Lagrangian approaches to multidimensional condensation and collection, J. Adv. Model. Earth Syst., 9, https://doi.org/10.1002/2017MS000930, 2017.

505 Liu, Q., Kogan, Y. L., Lilly, D. K., and Khairoutdinov, M. P.: Variational Optimization Method for Calculation of Cloud Drop Growth in an Eulerian Drop-Size Framework, J. Atmos. Sci, 54, https://doi.org/10.1175/1520-0469(1997)054<2493:VOMFCO>2.0.CO;2, 1997.

Margolin, L. G. and Shashkov, M.: MPDATA: gauge transformations, limiters and monotonicity, Int. J. Numer. Methods Fluids, https://doi.org/10.1002/fld.1070, 2006.

Margolin, L. G. and Smolarkiewicz, P. K.: Antidiffusive Velocities for Multipass Donor Cell Advection, SIAM J. Sci. Comput.,
510 https://doi.org/10.1137/S106482759324700X, 1998.

Margolin, L. G., Shashkov, M., and Smolarkiewicz, P. K.: A discrete operator calculus for finite difference approximations, Comput. Methods Appl. Mech. Eng., https://doi.org/10.1016/S0045-7825(00)80001-8, 2000.

Morrison, H., Witte, M., Bryan, G. H., Harrington, J. Y., and Lebo, Z. J.: Broadening of Modeled Cloud Droplet Spectra Using Bin Micro-
physics in an Eulerian Spatial Domain, J. Atmos. Sci, 75, https://doi.org/10.1175/JAS-D-18-0055.1, 2018.

515   Pardo, L. H., Morrison, H., Machado, L. A. T., Harrington, J. Y., and Lebo, Z. J.: Drop Size Distribution Broadening Mechanisms in a Bin
Microphysics Eulerian Model, J. Atmos. Sci., 77, https://doi.org/10.1175/JAS-D-20-0099.1, 2020.

Roberts, K. V. and Weiss, N. O.: Convective Difference Schemes, Math. Comput., 20, https://doi.org/10.2307/2003507, 1966.

Smolarkiewicz, P. K.: A simple positive definite advection scheme with small implicit diffusion, Mon. Weather Rev., 111,
https://doi.org/10.1175/1520-0493(1983)111<0479:ASPDAS>2.0.CO;2, 1983.

520   Smolarkiewicz, P. K.: A Fully Multidimensional Positive Definite Advection Transport Algorithm with Small Implicit Diffusion, J. Comp.
Phys., 54, https://doi.org/10.1016/0021-9991(84)90121-9, 1984.

Smolarkiewicz, P. K.: Multidimensional positive definite advection transport algorithm: an overview., Int. J. Numer. Methods Fluids, 50,
https://doi.org/doi:10.1002/fld.1071, 2006.

Smolarkiewicz, P. K. and Clark, T. L.: The multidimensional positive definite advection transport algorithm: Further development and appli-
525   cations, J. Comp. Phys., 67, https://doi.org/10.1016/0021-9991(86)90270-6, 1986.

Smolarkiewicz, P. K. and Grabowski, W. W.: The multidimensional positive definite advection transport algorithm: nonoscillatory option, J.
Comp. Phys, 86, https://doi.org/10.1016/0021-9991(90)90105-A, 1990.

Smolarkiewicz, P. K. and Margolin, L. G.: On Forward-in-Time Differencing for Fluids: Extension to a Curvilinear Framework, Mon.
Weather Rev., 121, https://doi.org/10.1175/1520-0493(1993)121<1847:OFITDF>2.0.CO;2, 1993.

530   Smolarkiewicz, P. K. and Margolin, L. G.: MPDATA – A multipass donor cell solver for geophysical flows, in: Godunov methods: Theory
and applications, edited by Toro, E., Springer, https://doi.org/10.1007/978-1-4615-0663-8_81, 2001.

Smolarkiewicz, P. K. and Rasch, P. J.: Monotone Advection on the Sphere: An Eulerian Versus Semi-Lagrangian Approach, J. Atmos Sci,
48, 1991.

Smolarkiewicz, P. K. and Szmelter, J.: MPDATA: An edge-based unstructured-grid formulation, J. Comp. Phys., 206,
535   https://doi.org/10.1016/j.jcp.2004.12.021, 2005.

Toro, E.: Riemann Solvers and Numerical Methods for Fluid Dynamics, Springer, 2 edn., https://doi.org/10.1007/b79761, 1999.

Tsang, T. H. and Brock, J. R.: Simulation of Condensation Aerosol Growth by Condensation and Evaporation, Aerosol Sci. Tech., 2,
https://doi.org/10.1080/02786828308958637, 1982.

Tsang, T. H. and Korgaonkar, N.: Effect of Evaporation on the Extinction Coefficient of an Aerosol Cloud, Aerosol Sci. Tech., 7,
540   https://doi.org/10.1080/02786828708959167, 1987.

Tsang, T. H. and Rao, A.: Comparison of Different Numerical Schemes for Condensational Growth of Aerosols, Aerosol Sci. Tech., 9,
https://doi.org/10.1080/02786828808959214, 1988.

Tsang, T. H. and Rao, A.: A moving finite element method for the population balance equation, Num. Meth. Fluids, 10,
https://doi.org/10.1002/fld.1650100704, 1990.

545   Waruszewski, M., Kühnlein, C., Pawlowska, H., and Smolarkiewicz, P. K.: MPDATA: Third-order accuracy for variable flows, J. Comput.
Phys, 359, https://doi.org/10.1016/j.jcp.2018.01.005, 2018.

Wei, L., Sun, J., Lei, H., Dong, L., and Hu, W.: A Lagrangian Advection Scheme for Solving Cloud Droplet Diffusion Growth, Atmosphere,
11, https://doi.org/10.3390/atmos11060632, 2020.

Williams, M. M. R. and Loyalka, S. K.: Aerosol Science: Theory and Practice, Pergamon, 1991.

550 Yang, F., Kollias, P., Shaw, R. A., and Vogelmann, A. M.: Cloud droplet size distribution broadening during diffusional growth: ripening amplified by deactivation and reactivation, Atmos. Chem. Phys., 18, https://doi.org/10.5194/acp-18-7313-2018, 2018.